A photonic crystal superlattice based on triangular lattice

Curtis W. Neff and Christopher J. Summers

School of Materials Science and Engineering
Georgia Institute of Technology, Atlanta, Georgia 30332-0245

curtis.neff@mse.gatech.edu

Abstract: A two-dimensional superlattice photonic crystal structure is investigated in which the holes in adjacent rows of a triangular lattice alternate between two different radii. The superimposition of a superlattice on a triangular lattice is shown to reduce the photonic bandgap, introduce band splitting, and change the dispersion contours so that dramatic effects are seen in the propagation, refraction, and dispersion properties of the structure. For single mode propagation, the superlattice shows regions of both positive and negative refraction as well as refraction at normal incidence. The physical mechanisms responsible for these effects are directly related to Brillouin Zone folding effects on the triangular lattice that lowers the lattice symmetry and introduces anisotropy in the lattice.

OCIS codes: (260.2110) Electromagnetic theory; (350.3950) Micro-optics

References and links

1. J. P. Dowling and C. Bowen, "Anomalous index of refraction in photonic bandgap materials," J. Mod. Opt. **41**, 345 (1994).
2. S.-Y. Lin, V. M. Hietala, L. Wang, and E. D. Jones, "Highly dispersive photonic band-gap prism," Opt. Lett. **21**, 1771 (1996).
3. H. Kosaka, T. Kawashima, A. Tomita, M. Notomi, T. Tamamura, T. Sato, and S. Kawakami, "Superprism phenomena in photonic crystals," Phys. Rev. B **58**, R10,096 (1998).
4. M. Notomi, "Theory of light propagating in strongly modulated photonic crystal: Refraction like behavior in the vicinity of the photonic band gap," Phys. Rev. B **62**(16), 10,696 (2000).
5. J. Bravo-Abad, T. Ochiai, and J. Sànchez-Dehesa, "Anomalous refractive properties of a two-dimensional photonic band-gap prism," Phys. Rev. B **67**, 115,116 (2003).
6. W. Park and C. J. Summers, "Extraordinary refraction and dispersion in two-dimensional photonic-crystal slabs," Opt. Lett. **27**(16), 1397 (2002).
7. H. Kosaka, T. Kawashima, A. Tomita, M. Notomi, T. Tamamura, T. Sato, and S. Kawakami, "Photonic crystals for micro lightwave circuits using wavelength-dependent angular beam steering," Appl. Phys. Lett. **74**(10), 1370 (1999).
8. L. Wu, M. Mazilu, T. Karle, and T. F. Krauss, "Superprism phenomena in planar photonic crystals," IEEE J. Quantum Electron. **38**(7), 915 (2002).
9. T. Baba and M. Nakamura, "Photonic crystal light deflection devices using the superprism effect," IEEE J. Quantum Electron. **38**(7), 909 (2002).
10. W. Park, J. S. King, C. W. Neff, C. Liddell, and C. J. Summers, "ZnS-based photonic crystals," Phys. Status Solidi B **229**(2), 949 (2002).
11. T. Baba and T. Matsumoto, "Resolution of photonic crystal superprism," Appl. Phys. Lett. **81**, 2325 (2002).
12. W. Park and C. J. Summers, "Optical properties of superlattice photonic crystal waveguides," Appl. Phys. Lett. **84**(12), 2013 (2004).
13. C. J. Summers, C. W. Neff, and W. Park, "Active Photonic Crystal Nano-Architectures," J. Nonlinear Optical Phys. and Mater. **12**(4), 587 (2003).
14. N. W. Ashcroft and N. D. Mermin, *Solid State Physics* (W. B. Saunders, 1976).

#6848 - $15.00 US Received 15 March 2005; revised 11 April 2005; accepted 12 April 2005

15. S. G. Johnson and J. D. Joannopoulos, "Block-iterative frequency-domain methods for Maxwell's equations in a planewave basis," Opt. Express **8**(3), 173 (2001).
16. A. J. Ward and J. B. Pendry, "A program for calculating photonic band structures and Green's functions using a non-orthogonal FDTD method," Comput. Phys. Commun. **112**(1), 23 (1998).
17. C. T. Chan, Q. L. Yu, and K. M. Ho, "Order-N spectral method for electromagnetic waves," Phys. Rev. B **51**(23), 16,635 (1995).
18. S. G. Johnson, S. Fan, P. R. Villeneuve, J. D. Joannopoulos, and L. A. Kolodziejski, "Guided modes in photonic crystal slabs," Phys. Rev. B **60**(8), 5751 (1999).
19. J. Berenger, "A perfectly matched layer for the absorption of electromagnetic waves," J. Comput. Phys. **114**, 185–200 (1994).
20. L. Zhao and A. Cangellaris, "GT-PML: generalized theory of perfectly matched layers and its application to the reflectionless truncation of finite-difference time-domain grids," IEEE Trans. Microwave Theory Tech. **44**, 2555–2563 (1996).
21. P. J. Russell and T. A. Birks, "Bloch wave optics in photonic crystals: physics and applications," in *Photonic band gap materials*, C. M. Soukoulis, ed., no. 315 in NATO ASI series. Series E, applied sciences, p. 71 (Kluwer, 1996).

1. Introduction

The dispersive properties of two-dimensional photonic crystals (2D PCs) are of great interest because of the potential they show for extraordinary refraction effects beyond the capabilities of conventional prisms and gratings [1, 2, 3, 4, 5, 6, 7] and their potential applications in optical systems such as wavelength-division multiplexing (WDM) [7, 8, 9]. In 1998, Koska *et al.* observed the *superprism effect* using a pseudo-2D 'autocloned' structure [3], and more recently, the superprism effect has been predicted [6, 10] and demonstrated [8] in 2D PC planar waveguide configurations. Wavelength dispersive effects in 2D PC structures suitable for WDM were confirmed by Wu *et al.* who showed a change of 10° in the incident beam refraction angle when the incident wavelength was scanned by 20 nm [8]. In 2002, Baba *et al.* quantified the resolution of the superprism effect in photonic crystals by introducing a resolutions parameter q/p where p represents the degree of beam divergence, $p = (\partial\theta_r/\partial\theta_i)$, and q represents the wavelength sensitivity, $q = \partial\theta_r/\partial(a/\lambda)$, where θ_r is the propagating beam angle in the PC, θ_i is the incident beam angle, a is the lattice constant, and λ is the freespace wavelength [11]. Through their analysis, they found that although the resolution of a superprism is sufficient ($q/p > 75$) to use in WDM systems, the effect in triangular lattice PCs is not strong enough to allow device structures smaller than 1 cm^2 [11]. Thus, alternate structures and PC configurations must be investigated for improvement in superprism performance.

In previous work, we reported a 2D PC triangular lattice whose holes were infiltrated with an electro-optic (EO) or nonlinear material (NL) so that an alternating bias of adjacent rows of the lattice imposed a superlattice (SL) modulation of their dielectric constants and introduced Brillouin zone (BZ) folding effects which improved the dynamic tunability of refraction in 2D PCs [12, 13]. In this work, we propose a new lattice configuration that incorporates two different hole radii, Fig. 1(a), to create a SL-PC structure that introduces a variety of unique optical phenomena such as positive *and* negative refraction at a *single excitation wavelength*, normal incidence refraction, and high dispersion: an order of magnitude greater than that predicted for the triangular lattice. The unit cell definition of the SL now consists of two holes per lattice point so that the basis vectors are orthogonal as opposed to being inclined at 60°, as in the triangular lattice. This new structure lowers the crystal symmetry through BZ folding and creates a strong interaction between the photonic dispersion surfaces. As a result the dispersion response becomes highly asymmetrical, thereby introducing significantly different phenomena than observed in either for triangular or square lattices.

#6848 - $15.00 US Received 15 March 2005; revised 11 April 2005; accepted 12 April 2005

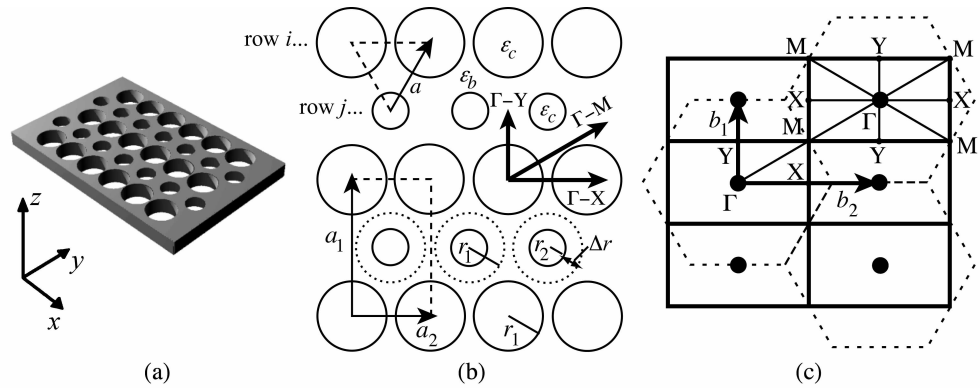

Fig. 1. Details of the SL structure.(a) An illustration of a SL slab waveguide. (b) A schematic showing the parameters of the structure. (c) Reciprocal lattice representation.

2. The superlattice structure

Figures 1(a) and 1(b) respectively, show an illustration of the SL-PC waveguide structure and a schematic that describes the parameters of the structure. The structure consists of a triangular lattice of circular holes (dotted triangle) of two different radii such that adjacent rows, i and j, consist of a single radius, r_1 or r_2, respectively. The $[i, j]$ rows introduce an additional periodicity in the lattice in the y-direction. To incorporate this additional periodicity, a Bravais lattice with a two-point basis is used so that the new basis vectors $\mathbf{a}_1 = a(0,\sqrt{3})$ and $\mathbf{a}_2 = a(1,0)$ define a rectangular unit cell, where a is the lattice constant of the underlying triangular lattice. As in solid-state physics, a monatomic lattice with an n-atom basis (in the present case $n = 2$ holes) introduces a structure factor, $S_{\mathbf{K}}$, given by

$$S_{\mathbf{K}} = \sum_{j=1}^{n} f_j(\mathbf{K}) e^{i\mathbf{K}\cdot\mathbf{d}_j}, \tag{1}$$

where $\mathbf{K}$ is a reciprocal lattice vector, f_j is the form factor, and $\mathbf{d}_j$ is the coordinate of the jth hole [14]. In the present discussion, the form factor is dependent upon the radius of the jth hole, i.e. identical holes have identical form factors. From $\mathbf{a}_1$ and $\mathbf{a}_2$, the primitive reciprocal lattice vectors are given by $\mathbf{b}_1 = (2\pi/a)(0, 1/\sqrt{3})$ and $\mathbf{b}_2 = (2\pi/a)(1,0)$, which also defines a rectangular area and is shown by the solid lines in Fig. 1(c) . Since any reciprocal lattice vector can be written as a linear combination of $\mathbf{b}_1$ and $\mathbf{b}_2$, a general expression for $\mathbf{K}$ is given by

$$\mathbf{K} = n_1\mathbf{b}_1 + n_2\mathbf{b}_2, \tag{2}$$

where n_1 and n_2 are integers. Substituting Eq. (2) into Eq. (1) and using $\mathbf{d}_1 = (0,0)$ and $\mathbf{d}_2 = (a/2)(\sqrt{3},1)$ gives

$$S_{\mathbf{K}} = f_1(\mathbf{K}) + (-1)^{n_1+n_2} f_2(\mathbf{K}). \tag{3}$$

If $r_1 = r_2$, Eq. (3) shows that the structure factor vanishes for those reciprocal lattice points whose coordinates are an odd sum with respect to the primitive vectors. This converts the rectangular reciprocal lattice into the hexagonal reciprocal lattice of triangular lattice which is indicated by the dotted lines in Fig. 1(c).

The new symmetry directions of the rectangular BZ are labeled in Fig. 1(c) and placed over the real lattice for reference in Fig. 1(b). As a consequence of the different shapes of the triangular lattice BZ and the SL BZ, those k-vectors that lie outside of the rectanglar BZ, but within

#6848 - $15.00 US Received 15 March 2005; revised 11 April 2005; accepted 12 April 2005

the hexagon of the triangular BZ are translated into the rectangle by a multiple of $\mathbf{b}_1$ and $\mathbf{b}_2$. Thus, these points are 'folded' back into the rectangular BZ, which is smaller and of lower symmetry [12, 13]. In total, there are now two equivalent X and Y points and four equivalent M points in the first BZ because of the SL. In addition, the irreducible BZ transforms from a triangle into a rectangle comprising 1/4 of the first BZ.

2.1. *Superlattice strength*

The strength of the SL modulation is controlled by $\Delta r = r_1 - r_2$ and is characterized by the radius ratio, r_2/r_1, which incorporates the relative sizes of the two holes. For the structures in this paper, r_1 was held constant at $0.35a$ while r_2 was decreased. Thus, as r_2/r_1 decreases, the SL strength, or modulation, increases. In a simplified approximation, the addition of dielectric material as r_2 is decreased can be used to calculate an effective ε for r_2 holes. For a pure 2D structure, this involves averaging the dielectric constant of the area of material added over the entire area of a r_1 hole. Assuming the additional material has the same dielectric constant as the background material, ε_b, the effective dielectric constant of a row j hole is given by

$$\varepsilon_{\mathrm{eff},j} = \varepsilon_b \left(1 - \left(\frac{r_2}{r_1}\right)^2\right) + \varepsilon_{c,i} \left(\frac{r_2}{r_1}\right)^2, \tag{4}$$

where $\varepsilon_{c,i}$ is the dielectric constant inside a row i hole. This equation shows that the magnitude of the dielectric modulation between rows is directly related to the difference between the hole sizes. For example, a change in radius of $\Delta_r = 0.05a$, from $r_1 = 0.35a$ to $r_2 = 0.3a$, corresponds to a r_1 hole with $\varepsilon_c = 3.918$, equivalent to an index change $\Delta n = 0.979$ between $[i, j]$ rows for $\varepsilon_b = 12$. Thus, radius modulated SLs with strengths $r_2/r_1 = 0.857$ and 0.571 introduce an index modulation equivalent to $\Delta n = 0.979$ and 1.90, respectively, between adjacent rows, clearly showing that the magnitude of the SL modulation is unprecedented in comparison to the previously reported SL which is limited by the NL properties of the material infiltrated into the holes [12, 13]. For this reason, the radius modulated SL is unique in its impact on this lattice structure. Naturally, the effective index method is an oversimplification, and it is included here for illustrative purposes and for comparison with the previously reported SL structure. Since it neglects the actual change in the dimensions of the dielectric/air interface for each hole, the effective index method was not employed in the calculations, but more appropriately, the hole radii were defined in the calculations to accurately model the SL structure.

3. Numerical results and discussion

For this study, band structures (ω vs. k relationships) and dispersion contours (k vs. k relationships) of the SL structure were calculated for both the pure 2D and the 2D slab waveguide configurations using numerical methods with periodic boundary conditions. For the pure 2D structures, a freely available plane wave expansion (PWE) software package was used because its speed of convergence and relatively low computational load allowed a detailed analysis of the entire k-space dispersion surface [15]. On the other hand a 3D finite difference time-domain (FDTD) code that was highly modified from that of Ward and Pendry was used to model the 2D slab waveguide structure [16, 17, 6]. A full 3D calculation was necessary because the finite thickness of the SL-PC slab waveguide structure introduces guided modes and light confinement effects [6, 18]. For both calculation methods, periodic boundary conditions were used in the x-y plane (see Fig. 1(a)) making them infinitely extended in these directions. In the z-direction, the PWE calculation assume that the holes and the slab were infinitely extended, while for the 3D FDTD calculations, the computational cell was truncated in the z-direction using a Berenger-type perfectly matched layer (PML) boundary condition on the top of the

#6848 - $15.00 US Received 15 March 2005; revised 11 April 2005; accepted 12 April 2005

cell and a mirror boundary condition on the bottom of the cell [19, 20]. The FDTD computational cell consisted of a dielectric slab adjacent to the mirror boundary followed by an air layer which leads into the PML. The placement of the mirror boundary allowed an increase in computational speed because it reduces the computational space by one half and allowed selection of even (TE-like) or odd (TM-like) modes according to their symmetry across the mirror plane.

For both structures, the slab dielectric was taken to be $\varepsilon_b = 12.0$ and the holes were air $\varepsilon_c = 1.0$. For the FDTD calculations, the slab waveguide was surrounded by air and the thickness was chosen to be $0.5a$, which allows single mode guiding while maintaining sufficient thickness for a high effective index of refraction of the slab. A slab that is too thin will have a lower effective index, thus increasing the frequency of the bands we are studying closer to the cutoff condition of the structure which is governed by the cladding, or in our case, the light line $\omega = ck$ [18]. Various radius ratios ranging from 1 to 0.571 were examined to observe the effect of the SL strength on the band structures and dispersion contours for the TE modes in the 2D SL-PC and TE-like modes in the 2D SL-PC slab waveguide. A similar analysis can be made for TM polarization where we have observed the same effects.

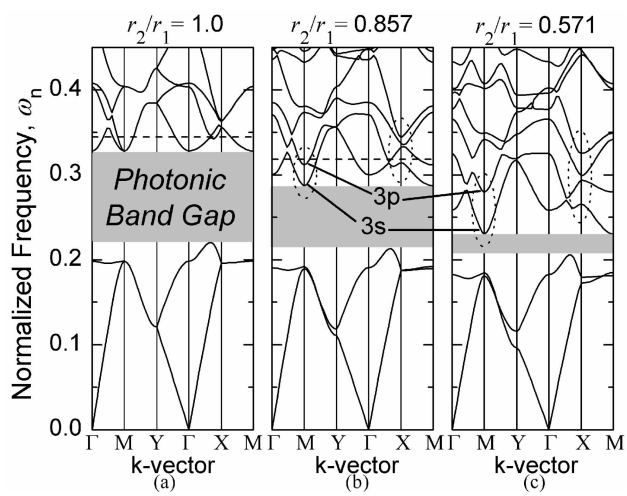

Fig. 2. Photonic band diagrams for SL structures calculated using the PWE method for (a) r_2/r_1=1.0, (b) 0.857, and (c) 0.571.

3.1. *Photonic band properties*

The results of the PWE calculations are presented in Figures 2(a), (b) and (c) which show the band structures for TE polarization with r_2/r_1 equal to unity, 0.857 and 0.571, respectively, for a constant $r_1 = 0.35a$. Similar results were obtained for the slab waveguide configuration with FDTD calculations. As expected, for $r_2/r_1 = 1$, the band structure was identical to the conventional triangular lattice after accounting for BZ-folding. However, the band structure is strongly affected by increasing the SL strength and several effects are predicted. The most pronounced is on the full PBG, which decreased rapidly as the SL strength is increased as indicated by the shaded boxes. For $r_2/r_1 = 0.875$ (0.571), the PBG was reduced in width by 31.5% (77.9%) for the 2D structure and by 30.6% (75.8%) for the slab waveguide. The second observation was that certain bands split into two states at many places in the BZ, some of which are highlighted by the dashed ellipses in Fig. 2(b) and (c). The separation of the two states is directly proportional to the SL strength and is related to the change in the distribution of electromagnetic (EM) energy as discussed below. The time-averaged energy density of the

#6848 - $15.00 US Received 15 March 2005; revised 11 April 2005; accepted 12 April 2005

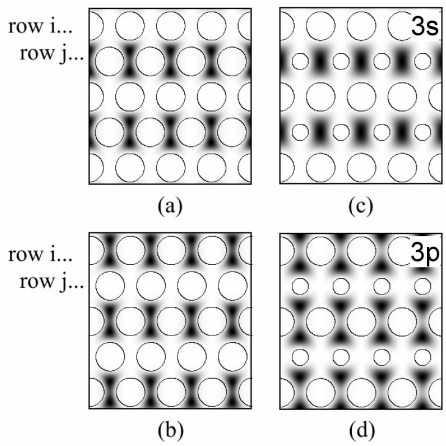

Fig. 3. Time-averaged magnetic-field energy density of the H_z field component for (a) and (b) the degenerate states at the bottom of the air band at the M point of the triangular lattice and (c) and (d) the 3s and 3p states of the 2D PC-SL with strength 0.571.

H_z component of the TE mode was calculated using PWE at the M point for each strength of the SL in Fig. 2. For the triangular lattice, Fig. 3(a) and (b) show the degenerate states at the bottom of the air band at the M point when the SL unit cell is applied to the lattice. The mode with field nodes located in row *i* is indistinguishable from the mode with nodes in row *j* and their energy distributions are equal. When the SL strength is increased, the symmetry of the triangular lattice is broken as r_2 decreases, resulting in the lifting of this degeneracy. As a consequence of the radius change, the dielectric area between row *j* holes increases causing the mode in row *j* to become more 's-type' in shape (in analogy with solid-state physics nomenclature), while the other mode (in row *i*) becomes more 'p-type', as shown in Fig. 3(c) and (d) for a SL strength of 0.571. Hence in Fig. 2 (b) and (c), the bands corresponding to these field patterns are labeled 3s and 3p where the numeral indicates the band number and the letter indicates the field mode shape. As shown in the band diagram, the 3s mode decreases in energy while 3p increases in energy as the SL strength is increased. Consequently, the smaller the hole size ratio, i.e. the stronger the SL modulation, the larger the separation of energy localization and subsequent band splitting.

3.2. Dispersion contours and refraction properties

Figure 4(a) compares the dispersion contours in the irreducible BZ for three SL-PC structures. The solid lines are the BZ folded contours of the triangular lattice at $\omega_n = 0.3445$. Notice that the contours must converge to a point on the BZ boundaries Y-M and X-M as shown in Fig. 4(a) to be consistent with the number of intersection points of the 3rd band with the constant frequency line (dashed line in Fig. 2(a)) along the directions Y-M and X-M. When the third band splits into two distinct states, 3s and 3p, with the increase in SL strength, two dispersion surfaces in *k*-space with modified curvatures are created. Consequently, the contours of these two bands have different shapes than the parent band of the original triangular lattice. This is shown by the dashed lines and scattered dots in Fig. 4(a), which are the contours at $\omega_n = 0.3185$ and 0.3783, respectively, for a 2D SL-PC and a slab waveguide SL-PC both with a strength of 0.857. The modification of the curvature is especially evident along the boundaries of the first BZ where the Bloch condition requires that the contours are continuous and smooth across the BZ boundary in an extended zone scheme. Therefore, the contours must intersect

#6848 - $15.00 US Received 15 March 2005; revised 11 April 2005; accepted 12 April 2005

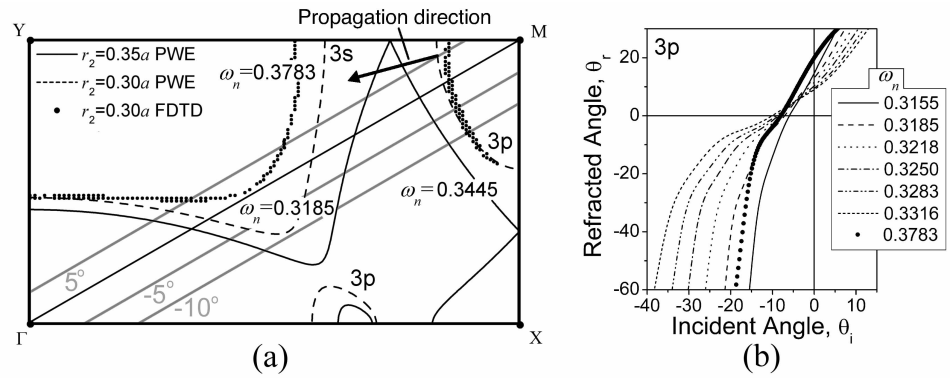

Fig. 4. (a) TE polarization equi-frequency contours for the SL structure calculated with the PWE method for a strength of 1.0 (solid line) and 0.857 (dashed line) and with the FDTD method for a radius ratio of 0.857 (scattered dots), gray lines indicate the construction lines for a beam of $\omega_n = 0.3185$ incident from air onto the PC. (b) Refraction angles with change in incident angle for $r_2/r_1 = 0.857$ for a range of ω_n with 1% spacing between frequencies (group of lines) and for a 2D slab waveguide structure (scattered plot).

the BZ boundary at a 90° angle resulting in a strong, local modification of the curvature as it approaches the Y-M and X-M boundaries. As a consequence, the contours appear to 'repel' one another along the BZ boundary in direct proportion to the strength of the SL modulation, rather than converge to a single point as in the unmodulated structure. Thus, the optical properties of a SL PC can be tailored to a specific application by adjusting the SL strength.

The combination of the symmetry reduction, the band splitting, and the continuity condition results in contours with highly modified curvatures, especially near the BZ boundaries, which gives rise to unique optical effects. Fig. 4(b) presents the results of wave-vector analysis on the dispersion contours from the 3p band of the 2D and the slab waveguide SL-PC when the contours in the upper right hand corner of the BZ radiating from the M point in Fig. 4(a) are used to calculate the direction of the Poynting vector [21]. The excitation beam is incident on the PC from air and is taken to be parallel to the Γ–M direction, and the gray construction lines indicate the conservation of the tangential component of the wave-vector, $k_{\parallel}$, across the air/PC interface at $\omega_n = 0.3185$ as the incident angle, θ_i, of the beam is increased in a positive (counter-clockwise) or negative (clockwise) manner. As θ_i is increased, the construction lines intersect the contour closer to the BZ boundary where the curvature modification is highest. Since the Poynting vector is normal to the contour surface at these intersections, the high curvatures at these points show that light will be strongly refracted as shown in Fig. 4(b). In this figure, the group of solid and dashed lines represent refraction in a 2D SL-PC structure at various ω_n -values spaced 1% in frequency, while the dotted curve is from a slab waveguide SL-PC at $\omega_n = 0.3783$. The SL-PCs presented in Fig. 4(a) are highly dispersive at θ_i larger than $-15°$. For example, for the SL strength shown, a 1% change in ω_n produces a 34° change in refracted angle, $\Delta\theta_r$, for $\theta_i = -15°$. This frequency dispersion increases with increase in SL strength as seen for $r_2/r_1 = 0.571$ where a 1% change in frequency ($\omega_n = 0.2805$ to 0.2833) produces $\Delta\theta_r = 65°$ at $\theta_i = 6.5°$. Also, giant refraction effects are observed in the SL-PCs in which an incident beam can be steered over a wide range of angles for a small change in incident angle, thus producing a very large steering coefficient $\Delta\theta_r/\Delta\theta_i$. For the contours plotted in Fig. 4(a), the 2D SL-PC structure shows $\Delta\theta_r = 70°$ when θ_i is increased from 0° to 15° at $\omega_n = 0.3155$ for a $\Delta\theta_r/\Delta\theta_i = 4.67$. The slab waveguide structure shows a comparable response at $\omega_n = 0.3783$

#6848 - $15.00 US Received 15 March 2005; revised 11 April 2005; accepted 12 April 2005

with $\Delta\theta_r/\Delta\theta_i = 4.11$, which steers the refracted beam $> 78^\circ$ for $\Delta\theta_i \sim 19^\circ$. Increasing the SL strength to 0.571 increases this effect to $\Delta\theta_r/\Delta\theta_i = 12.15$ at $\omega_n = 0.2805$ in the 2D structure which produces a beam steering $> 79^\circ$ for $\Delta\theta_i = -6.5^\circ$.

In addition to large superprism and giant refraction effects, as demonstrated earlier, the SL-PC shows unique refraction regimes in comparison to the triangular lattice. For instance, the refraction response of the triangular lattice is symmetric around high symmetry directions with no refraction at normal incidence [4, 6, 10]. This is the case for refraction calculated using the solid curve in the upper right corner of the BZ in Fig. 4(a) which is relatively flat and intersects the Γ–M line at a 90° angle. However, in a SL-PC with a strength of 0.857, the curvature of this contour is dramatically modified and is no longer normal to the Γ–M direction and is now asymmetric. Consequently, a beam at normal incidence will be refracted as shown in Fig. 4(b) for all of the refraction curves at θ_i=0. For example, a beam of frequency $\omega_n = 0.3155$ normally incident on a 2D SL-PC with strength 0.857 will be refracted 15°, and in a SL-PC slab waveguide of the same strength this value is almost 20° at $\omega_n = 0.3783$. In addition, the asymmetry of the contour about the Γ–M direction creates a refraction response that changes from positive refraction to negative then back to positive as θ_i is increased from -40° to $+15^\circ$. Again, this is a unique refraction response than what is reported in the triangular and square lattices where there is only a single refraction regime (either positive or negative) depending on the constant frequency chosen.

4. Conclusion

We have introduced a new superlattice photonic crystal structure in which alternating rows of holes of different radii create an additional modulation in the lattice. This structure introduces a wide range of new phenomena by providing the ability to manipulate the photonic dispersion surfaces with a high degree of control, thereby redefining the optical response (propagation, refraction, and dispersion) of 2D PCs. The addition of this lattice design parameter greatly increases the functionality and flexibility of PCs in optical systems and allows for a greater strength in the SL modulation, defined by the radius ratio, r_2/r_1. Unique phenomena are observed in this structure such as (1) normal incidence refraction, (2) highly asymmetrical refractive properties that produce regions of positive and negative refraction that are strongly dependent on θ_i, and (3) extremely large refraction ($\Delta\theta_r/\Delta\theta_i = 12.15$) and dispersion ($4^\circ$/nm at $1.55\mu m$) that will enable smaller device geometries for WDM, beam steering, and micro-spectrometer applications through the larger resolution parameter q/p that can be potentially enhanced an order of magnitude larger by further optimization of the structure. Additionally, the introduction of EO and/or NL materials into the lattice will provide yet another degree of design freedom and the ability to dynamically control the optical properties of devices incorporating the SL structure.

Acknowledgements

We wish to thank W. Park and T. Yamashita for valuable discussions and the Army Research Office for support under MURI Grant No. DAAD19-01-1-0603.